# UC Berkeley

### Title

Holographic Quantum Simulation of Entanglement Renormalization Circuits

### Permalink

https://escholarship.org/uc/item/8283t23d

### Journal

### ISSN

### Authors

Anand, Sajant
Hauschild, Johannes
Zhang, Yuxuan
et al.

### Publication Date

2023-09-01

### DOI

### Copyright Information

Peer reviewed

# Holographic Quantum Simulation of Entanglement Renormalization Circuits

Sajant Anand⬤,[1,*] Johannes Hauschild⬤,[1] Yuxuan Zhang⬤,[2] Andrew C. Potter,[3] and
Michael P. Zaletel[1,4,†]

[1]*Department of Physics, University of California, Berkeley, California 94720, USA*

[2]*Department of Physics, University of Texas at Austin, Austin, Texas 78712, USA*

[3]*Department of Physics and Astronomy, and Stewart Blusson Quantum Matter Institute, University of British
Columbia, Vancouver, British Columbia V6T 1Z1, Canada*

[4]*Material Science Division, Lawrence Berkeley National Laboratory, Berkeley, California 94720, USA*

While standard approaches to quantum simulation require a number of qubits proportional to the number of simulated particles, current noisy quantum computers are limited to tens of qubits. With the technique of holographic quantum simulation, a $D$-dimensional system can be simulated with a $(D-1)$-dimensional subset of qubits, enabling the study of systems significantly larger than current quantum computers. Using circuits derived from the multiscale entanglement renormalization ansatz (MERA), we accurately prepare the ground state of an $L = 32$ critical, nonintegrable perturbed Ising model and measure long-range correlations on the ten-qubit Quantinuum trapped-ion computer. We introduce generalized MERA networks that interpolate between MERA and matrix product state networks and demonstrate that generalized MERA can capture far longer correlations than a MERA with the same number of qubits, at the expense of greater circuit depth. Finally, we perform noisy simulations of these two network ansatzes and find that the optimal choice of network depends on the noise level, available qubits, and the state to be represented.

## I. INTRODUCTION

Simulations of strongly correlated quantum many-body physics relevant to materials science, chemistry, and fundamental physics are promising early applications of quantum computers [1]. An important task is to approximately prepare the ground state of a given system and measure its properties. Ground-state preparation is also a prerequisite for exploring near-equilibrium quantum dynamics of transport and ac responses. Standard approaches to quantum simulation directly encode each spin or electron orbital into a distinct hardware qubit, restricting the accessible problem size to the available qubit number. The paradigm of *holographic quantum simulation* provides an alternative for simulating a system of $n$ sites with less than $n$ qubits. Here, selected qubits are regularly measured, reset, and reused throughout the computation, and correlations between different physical sites are mediated by unmeasured qubits [2–6]. This allows a $D$-dimensional system to be simulated on a quantum computer with only enough hardware qubits to store the state of a $(D-1)$-dimensional cross section [7]. Formally, these techniques can be understood as a quantum compression of states into matrix product state (MPS) or tensor network state (TNS) form [2,5,6].

MPS [8] provide an efficient representation of one-dimensional (1D) states with area-law entanglement, with an accuracy that improves with the rank of the tensors $\chi$ faster than any power law [9,10]. The classical cost of MPS algorithms scales as $\mathcal{O}(\chi^2)$ for storage and $\mathcal{O}(\chi^3)$ for time, with $\chi$ growing exponentially with the bipartite entanglement entropy $S$. While tractable for most gapped 1D ground states, when simulating quantum dynamics or strips of $(D > 1)$-dimensional models, $S$ grows linearly in time or cross-sectional area, quickly making classical simulations prohibitive. The holographic approach for quantum simulation of an MPS requires only $1 + \log_2(\chi) \sim \mathcal{O}(S)$ qubits, an exponential reduction in storage. The time cost, however, is more subtle to assess, since holographically preparing a *generic* MPS requires acting with a $\chi \times \chi$ unitary that must be broken into a very deep circuit of gates. This obstacle motivated recent work [11–15]

to investigate the variational power of MPS and 2D TNS with tensors generated by finite-depth quantum circuits, dubbed quantum MPS (QMPS) and quantum TNS, respectively. It has been found that such circuits provide an efficient parameterization for approximating interesting physical states, sometimes even representing states with fewer variational parameters than their generic (dense) tensor network counterpart without sacrificing accuracy. Additionally, for 1D systems, ground-state optimization for correlated spin [6] and electron [16] systems, time evolution [13,17], and many-body entanglement measurements [18] were demonstrated experimentally on trapped-ion and superconducting qubit devices using holographic simulation of QMPS.

While finite-$\chi$ MPS can faithfully represent ground states of thermodynamically large 1D gapped systems [10], the natural tensor network for 1D critical systems is the multiscale entanglement renormalization ansatz (MERA), which can capture the power-law decay of critical correlations and the critical scaling of the entanglement entropy $S(L) \sim \log(L)$ of a subsystem of size $L$ [19–22]. While MPS and MERAs for 1D critical states both require a number of qubits that grows logarithmically with the system size to account for the growth in entanglement, MERAs are exponentially more sparsely parameterized than MPS, due to the inherent tree structure, and thus avoid the blowup in the quantum gate count.

In this work, we holographically prepare a generalization of the MERA representing critical, nonintegrable ground states on Quantinuum's System Model H1 trapped-ion quantum computer [23]. We find that increasing the MERA depth leads to measurable improvements in the observed long-range correlations. We discuss an enlarged class of generalized MERAs that provides a natural interpolation between MERA and MPS networks. We holographically prepare the generalized MERA and demonstrate that quantum correlations can be accurately measured, even using a low-depth network. Finally, we discuss the merits of these two networks in the presence of varying levels of noise.

## II. HOLOGRAPHIC SIMULATIONS OF MERA AND GENERALIZED MERA

There are two routes for holographically simulating a MERA. The first is to prepare a local patch of the desired state in a "top-down" approach [24]. As any local subset of sites in a MERA exhibit a bounded past causal cone, i.e., the set of tensors at each scale that can affect the subset, one can prepare the subset's reduced density matrix by viewing the MERA as a fine-graining quantum channel. Starting from fixed input states, one repeatedly applies the gates of the MERA, discarding and reusing those that exit the bounded causal cone of the desired patch. After sufficient iterations, the state of the qubits will approach

the fixed point of the quantum channel, even with noisy gate operations. This approach was recently demonstrated on a trapped-ion quantum computer [25], finding that such circuits are robust to noise as theoretically predicted in Ref. [24].

The second method is to view the MERA "sideways" as a circuit for preparing each site in turn, effectively trading the space and time directions. As in holographic simulations of QMPS, bond qubits carry correlations between sites represented by a physical qubit. Analogous theoretical guarantees of noise robustness as in the top-down approach cannot be made, as the circuit is not used to prepare fixed points of the quantum channel. As discussed later, however, we find such circuits to be remarkably resilient to noise.

We focus on binary MERAs as shown in Fig. 1(a), where each layer consists of both a row of disentangling unitaries and coarse-graining isometries that halve the degrees of freedom [20,21,26]. While MERAs are often used in their scale-invariant formulation with a single layer repeated indefinitely, the number of available qubits limits a sideways holographic simulation to MERAs with a finite depth of $d$ layers. Such networks have a finite support for correlations, growing exponentially with $d$; the maximum range $r_d$ of nonzero correlations in the bulk is given by the recursion relation

$$r_d = 2r_{d-1} + 2 \quad \text{with } r_0 = 1. \tag{1}$$

Note that, while doubling the range of correlations, each additional layer in the MERA requires only roughly half the number of tensors as the previous, leading to a total number of $\sum_{j=1}^{d} (L/2^{j-1} - 1) < 2L$ tensors for a lattice of $L = 2^n$ sites.

### A. Quantum circuit implementation

Given an optimized binary MERA representing a state that we wish to holographically prepare, we first reshape the network to the *isometric* form shown in Fig. 1(b). This is accomplished simply by bending the legs of the diagram so that the isometric arrows point down and to the right and is done to be consistent with the generalized MERA networks we discuss later. To prepare the state on a quantum computer, we extend the isometries with orthogonal columns into square unitary matrices representing by gates acting on a physical qubit and ancilla bond qubits. When extending an isometry, the added legs act on a fixed reference state, $|0\rangle$, as shown in Fig. 1(b). The circuit propagates along the direction of the arrows [27], so the leftmost site is prepared first starting with $|0\rangle$ initialized qubits and acting with the gates specified by the tensors moving down the leftmost column. Once all tensors in the column have been used, we can measure the physical qubit in the desired basis and proceed to the next site.
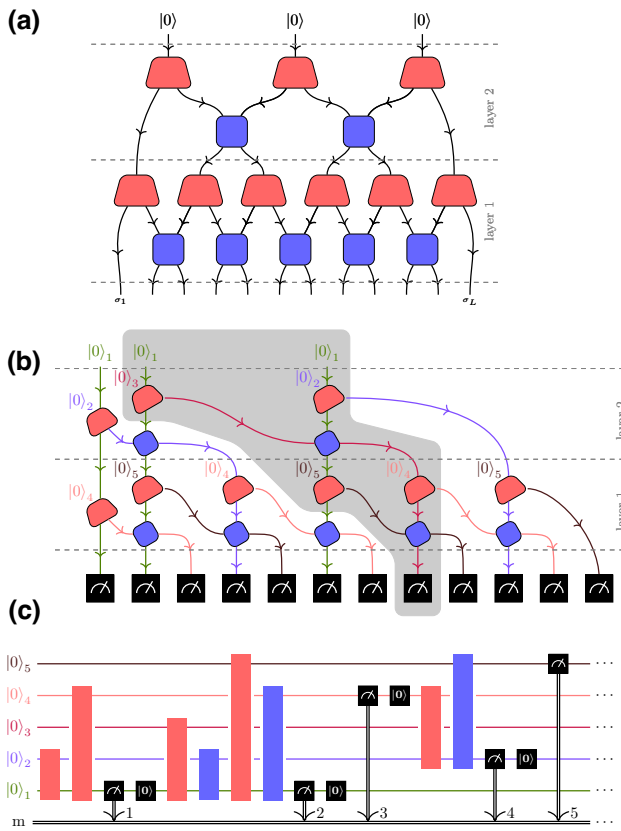
FIG. 1. Holographic simulation of a MERA. (a) Depth-2 MERA network structure for a spin chain of 12 sites consisting of alternating sublayers of two-site unitaries (blue) and isometries (red). (b) Isometric representation for the MERA formed by bending the wires. Five qubits, which are color coded, are required for holographic simulation. Arrows indicate the flow of time in the quantum circuit. The causal cone for site 8 is shaded in gray, and the number of tensors in the causal cone is independent of the length $L$ of the state. (c) Quantum circuit for the first five sites corresponding to the MERA network. Each isometry has been enlarged to a two-qubit unitary, and midcircuit measurements and resets are shown explicitly.

Once measured, the physical qubit can be reset to $|0\rangle$ and reused in other parts of the circuit, as depicted in Fig. 1(c).

For a bond dimension $\chi$ MERA, each gate acts on $2 \log_2 \chi$ qubits, so we require $\chi = 2$ to work with two-site gates. Hence, a depth-$d$, $\chi = 2$ MERA circuit requires $2d + 1$ qubits, which can be intuitively understood as one qubit for each isometric and unitary sublayer and one physical qubit. For implementation on quantum computers with a limited two-qubit gate set, we decompose each two-qubit $U(4)$ gate into a sequence of seven single-qubit rotations specified by 15 angles and three controlled-NOT (CNOT) gates, ignoring an irrelevant global phase [28].

The causal cone of a MERA has bounded width, as shown in Fig. 1(b). The causal cone for binary MERA saturates to width 3 after a few coarse-graining layers, so six

qubits are sufficient to evaluate up to next-nearest-neighbor operators for the top-down holographic method regardless of circuit depth $d$. Generic $n$-point functions will require $6n$ qubits, as $n$ disjoint causal cones must be maintained until they merge. The sideways holographic approach uses fixed $2d + 1$ qubits to evaluate arbitrary operators, as each site is prepared sequentially. Hence, evaluation of correlation functions as a function of distance between operators is more naturally implemented on qubit-limited devices using the sideways methods.

As holographic simulation enables preparation of the parameterized tensor network on the quantum hardware and measurement of all desired expectation values, one can imagine an optimization scheme where one iteratively adjusts parameters of the network and measures the energy as the cost function to be minimized directly on the quantum hardware [3,14,29]. The sideways approach to holographic MERA simulation lends itself to such optimization, since, for the example of the transverse-field Ising model discussed later, two iterations of the circuit, measuring once in the $X$ basis and once in the $Z$ basis, are sufficient to determine the energy and all $N$-point $X$ and $Z$ correlations, even in spatially inhomogeneous systems. An iteration of a sideways MERA circuit requires at most $2L$ gates for a maximum depth circuit. For the top-down method, preparing each site requires approximately $5d$ gates, yielding a total gate cost of $5dL$.

### B. Generalized MERA

The finite support of correlations inherent in a MERA motivates us to consider an alternate ansatz that we call the generalized MERA. As illustrated in Fig. 2, each layer of this network can be viewed as a coarse-graining matrix product operator, first introduced in the context of MPS renormalization [30]. The generalized MERA interpolates between the MERA and circuits composed of ladder unitary layers that form a simple implementation of QMPS (we consider such ladder circuits in Appendix C). Any MERA with bond dimension $\chi$ can also be represented by a generalized MERA with the same vertical bond dimension by simply replacing selected gates in Fig. 2 with identity operations to produce the circuit shown in Fig. 1(b). The generalized MERA corresponds to switching from a brick-wall pattern of unitaries used in the MERA to a ladder pattern, so already a single layer of unitaries has an infinite support of correlations [13]. Yet, correlations of a single layer still decay exponentially as for MPS [30]. Furthermore, we note that even $\chi > 2$ binary MERA can be represented by a generalized MERA with vertical bond dimension 2 but horizontal bond dimension $\chi^2/2$.

Like the regular MERA, a $\chi = 2$ generalized MERA with $d$ layers requires $2d + 1$ qubits in a holographic simulation, which again can be performed column by column as before. For a lattice of $L = 2^n$ sites, a depth $d$ generalized
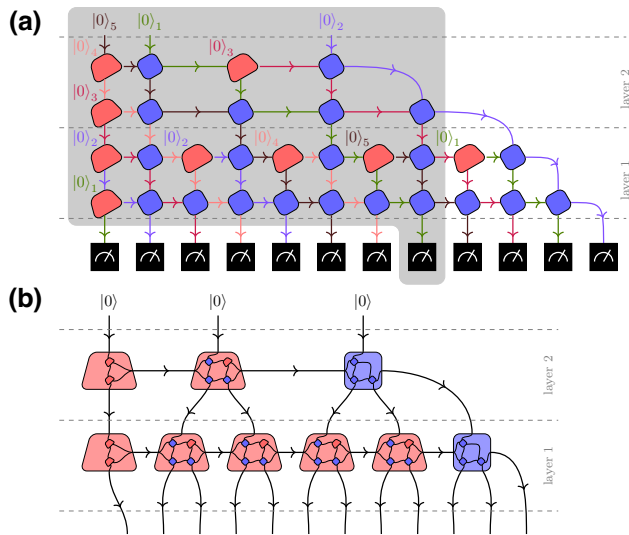
FIG. 2. (a) Isometric representation for the generalized MERA structure of depth 2 for a chain of 12 sites. Five qubits, which are color coded, are required for holographic simulation. The red and blue tensors are isometries and unitaries, respectively. The causal cone for site 8 is shaded in gray, and for a state of length $L$, there are $\mathcal{O}(L)$ tensors in the causal cone, regardless of depth. (b) By grouping tensors from the isometric and unitary sublayers, each layer of the generalized MERA can be seen as a coarse-graining matrix product operator [30].

MERA requires $\sum_{j=1}^{d}(L/2^{j-2} - 3) < 4L$ arbitrary two-qubit gates, roughly twice as many as the MERA. This additional gate cost is contrasted with the infinite support of correlations even with a single generalized MERA layer. As can be seen in Fig. 2, the causal cone for any site includes all tensors up and to the left and is thus extensive. Top-down simulations are not feasible for generalized MERA circuits, as the required number of qubits depends on both $d$ and $L$.

We note that we could instead consider MERA and generalized MERA networks with $\chi > 2$ and instead parameterize each tensor in terms of a sequence of two-qubit gates. A recent study found QMPS tensors parameterized in this way to, at times, provide a more efficient while equally accurate representation of the ground state than dense MPS tensors of dimension $\chi \times D \times \chi$, where $D$ is the physical Hilbert space dimension [12].

## III. HARDWARE IMPLEMENTATION

To demonstrate the ability of quantum circuits generated from MERA and generalized MERA to accurately capture quantum correlations using these holographic simulation methods, we study the spin-1/2 transverse-field Ising (TFI) model with a *self-dual* perturbation:

$$H = \sum_i -(X_iX_{i+1} + Z_i) + V(Z_iZ_{i+1} + X_iX_{i+2}) \quad (2)$$

with $X_i, Z_i$ the spin-$\frac{1}{2}$ Pauli operators on site $i$. The first term is the critical TFI model that is integrable. To break integrability, we add a self-dual coupling, which, under the Kramers-Wannier duality $X_iX_{i+1} \rightarrow \tilde{Z}_i, Z_i \rightarrow \tilde{X}_i\tilde{X}_{i+1}$, maps to itself [31]. Coupling $V \approx 250$ corresponds to the tricritical point described by the tricritical Ising conformal field theory (CFT) with central charge $c = 7/10$. Values $-0.28 < V < 250$ correspond to critical, nonintegrable perturbations to the critical Ising CFT with usual central charge $c = 1/2$ [32]. In our experiments and simulations, we use $V = 4$ to maximize the magnitude of the oscillations of $XX$ correlation functions.

Holographic simulation requires the ability to address, measure, and reset individual qubits throughout the quantum circuit and is thus naturally suited to trapped-ion devices. We run our circuits on the Quantinuum's System Model H1 quantum computer, with ten $^{171}$Yb$^+$ hyperfine qubits and a quantum volume of 64 [23]. Given that a depth-$d$ MERA or a depth-$d$ generalized MERA requires $2d + 1$ qubits, we can prepare at most a depth-4 network using nine qubits for a lattice of arbitrary size. Such depth is sufficient for a MERA network to have nonzero correlations over a range of 46 sites. While we could use the quantum computer to variationally optimize the tensor networks based on energy minimization, as discussed in Sec. II, in this work we instead optimize the tensor networks with classical computers to reduce the quantum hardware cost. This involves first finding an "exact" representation of the state as a large bond-dimension MPS and then iteratively converting it to the desired MERA or generalized MERA; see Appendix A for details on how we determine the classical tensor networks and convert the tensors into two-qubit gates. A similar approach of decomposing MPS into brick-wall and sequential quantum circuits have been considered [33,34].

We prepared $L = 32$ ground states of the self-dual Ising model in Eq. (2) as depth $d = 1, 2, 3, 4$ MERAs and depth $d = 1, 2$ generalized MERAs on the H1 quantum processor and measured all sites in the $X$ basis, extracting both on-site expectation value $\langle X_i \rangle$ and connected two-point correlation $C_X(10, r) = \langle X_{10}X_{10+r} \rangle - \langle X_{10} \rangle\langle X_{10+r} \rangle$. Here, $i = 10$ is chosen sufficiently within the bulk of our $L = 32$ system to minimize boundary effects and to also reach the maximal support of nonzero correlations for depth $d = 1, 2, 3$ MERAs. For each MERA (generalized MERA), we obtained at least $N_S = 2000$ ($N_S = 1000$) samples of measurement bitstrings, which yielded expectation values and correlation functions simultaneously. Additional experimental details can be found in Appendix B.

The results are shown in Fig. 3. We observe that increasing the depth of the MERA clearly extends the range of correlations we can capture, as the finite correlation support at low depth $d$ is clearly a severe limitation. In stark contrast, any generalized MERA will have nonzero, exponentially decaying correlations between any two sites, and
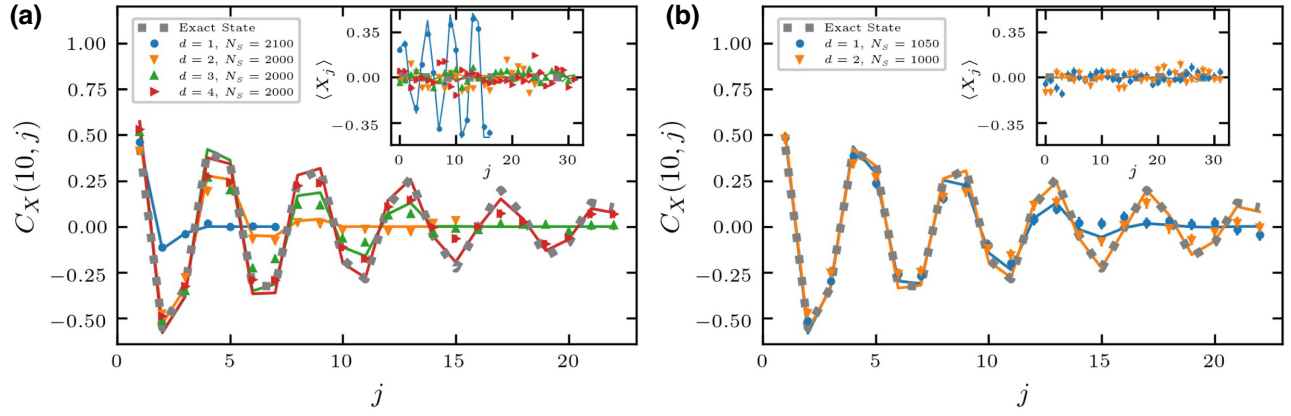
FIG. 3.   Connected $XX$ correlations $C_X(10,j)$ for an $L = 32$ $H_{\text{TFI-SD}}$ chain. In both plots, solid lines are the exact tensor network results for the MERA and generalized MERA at depth $d$, while dots with error bars are from $N_S$ measurement shots on the Quantinuum H1 computer for (a) MERA and (b) generalized MERA networks of varying depth $d$. The dashed gray line is the "exact" result given by the large bond-dimension MPS that we use to generate the MERA and generalized MERA networks and quantum circuits. Insets show $\langle X \rangle$ for the same networks. We simulate up to site 17 for the depth-1 MERA, up to site 25 for depth 2, and the entire chain for depth-3 and depth-4 MERAs and depth-1 and depth-2 generalized MERAs.

we find that even a depth-($d = 1$) generalized MERA can capture the correlations fairly accurately over a wide range of sites much larger than the range $r_1 = 4$ of the nonzero MERA correlations. A depth-$d$ MERA uses approximately as many gates as a depth-$d/2$ generalized MERA and twice as many qubits, and for this short chain, we see that both the $d = 4$ MERA and $d = 2$ generalized MERA can sufficiently capture correlations over the length of the chain.

## IV. NOISE ANALYSIS

We have shown experimentally that additional layers in either the MERA or generalized MERA network allow us to more accurately capture correlations between distant sites, as the network ansatz becomes more expressive. Additional layers, however, incur a cost of an increased number of two-qubit arbitrary unitary gates that must be performed, which leads to a larger negative effect of gate noise.

To investigate the trade-off between network depth and performance on noisy quantum computers, we perform noisy simulations of MERAs and generalized MERAs of an $L = 256$ unperturbed TFI model [Eq. (2) with $V = 0$] [35] ground state and measure $C_X(66,r)$, as shown in Fig. 4. We study MERAs of depth up to 7—reducing the sites in the lattice from 256 sites down to 2—and generalized MERAs up to depth 3, where additional depths only lead to marginal improvements in the correlations; additional results for unitary networks formed entirely of ladder unitary sublayers of generalized MERAs are discussed in Appendix C. Noisy circuit simulations are performed with Qiskit [36], using $10^4$ measurement shots per data point, and with depolarizing errors $E(\rho_n) = (1 - p_n^{\text{err}})\rho + p_n^{\text{err}}\mathbb{1}/2^n$ applied to all one- and two-qubit gates with

depolarizing rates $p_{1,2}^{\text{err}}$, respectively. On the Quantinuum processor, the error rates measured by randomized benchmarking were $p_1^{\text{err}} = 1.1 \times 10^{-4}$ and $p_2^{\text{err}} = 7.9 \times 10^{-3}$ [23]. In simulations, we vary the one-qubit error rate and fix the ratio between one- and two-qubit error rates to $p_2^{\text{err}} \equiv 10\,p_1^{\text{err}}$.

From the simulations shown in Fig. 4, we find that, for the three noise levels shown, there is always an improvement in the measured correlations by increasing the depth of the MERA circuit. This is because the added benefit of a more expressive ansatz with a longer range of nonzero correlations outweighs the added noise of additional gates; especially between a $d = 6$ and $d = 7$ network, the additional layer allows us to accurately capture correlations across the length of the chain while adding only three additional gates.

For the generalized MERA, where already a depth-($d = 1$) network can accurately capture correlations up to approximately 30 sites at large noise levels, we expect additional layers to be more impacted by noise than additional MERA layers. A depth-$d$ generalized MERA uses approximately twice as many arbitrary two-qubit unitaries as a depth-$d$ MERA. Additionally, noisy tensors in isometric networks can only affect the tensors in their future causal cone. For the MERA, the extent of the future causal cone of each tensor is finite and is governed by the recursion relation given earlier in Eq. (1); for the generalized MERA, the future causal cone of each tensor is extensive, and thus an error at site $i$ will affect all sites $j > i$. Such effects can be seen in Fig. 4, where the performance of higher-depth generalized MERAs is strongly dependent on the noise level, unlike that of high-depth MERAs. This is consistent with previous analysis of the top-down holographic MERA approach, which was shown
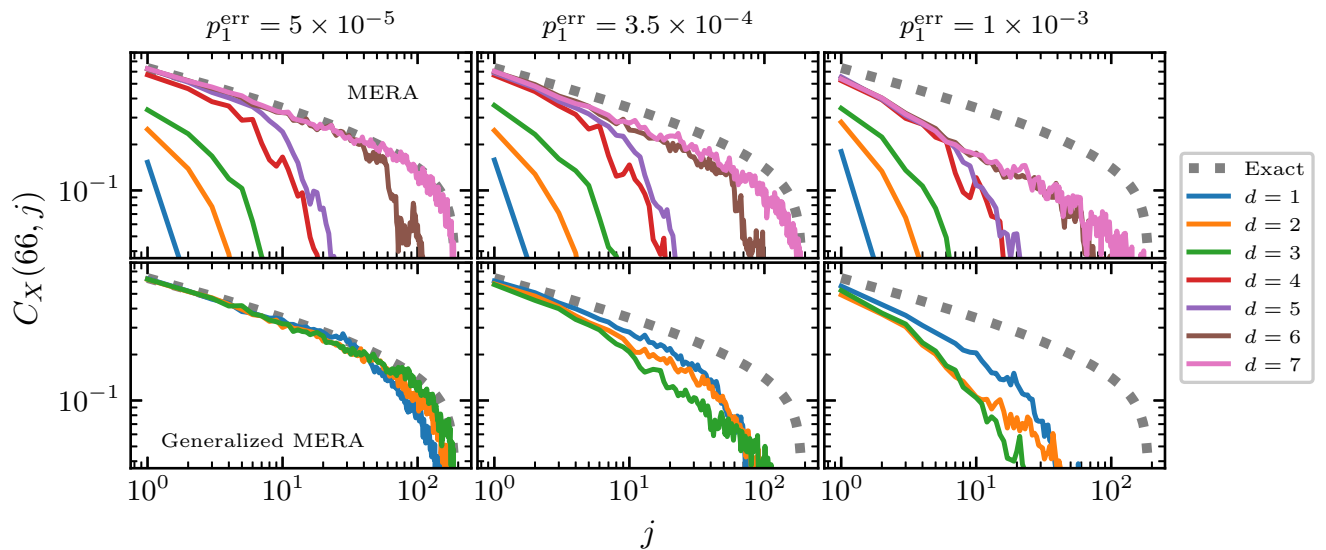
FIG. 4. Simulations of $L = 256$ ground states for the unperturbed TFI model realized by MERA (top row) and generalized MERA (bottom) networks for different probabilities of depolarizing noise and network depths. Two-qubit error rates are chosen as $p_2^{\mathrm{err}} = 10p_1^{\mathrm{err}}$. For both networks of depth $d$, the required number of qubits for holographic simulation is $2d + 1$, indicating that the low-depth generalized MERA can capture longer correlations than same depth MERA counterparts, even in the large noise limit. Simulations require only up to 15 qubits and are thus tractable on classical computers, despite being for an $L = 256$ spin chain.

both theoretically and experimentally to be noise resilient [24,25].

For MERA, across all noise levels, one should choose the minimum depth network—in order to minimize qubit and gate costs—that reproduces the noiseless correlations on the desired scale and to the desired accuracy; empirically, we see that even with high noise rates a depth-$d$ MERA more accurately captures correlations across all scales than networks with fewer layers. For generalized MERAs, the error rate fixes an optimal depth that minimizes the correlation errors; for example, in Fig. 4, for correlations between sites separated by a distance of 100, at low noise level the depth-3 generalized MERA is most accurate, while at high noise levels the accumulated noise from extensive future causal cones leads to the depth-1 generalized MERA being optimal. We note, however, that at all noise levels the depth-$d$ generalized MERA performs better than the MERA of the same depth and number of qubits, as the benefit of an infinite range of correlations far outweighs the increased susceptibility to noise. When, as is typically the case, the simulations are limited by the number of available qubits, the generalized MERA is hence a better choice, even in the presence of significant noise. We note that all of the investigated circuits are derived from tensor networks optimized without noise, so it is an open question if better performance can be achieved by optimizing a circuit for a particular $p_{\mathrm{err}}$.

## V. CONCLUSION

In this work, we have accurately measured long-range correlations in the ground state of a nonintegrable critical 1D system represented by MERA and generalized MERA

networks. We demonstrated that increasing the depth of the network directly improved the correlations measured. The generalized MERA network interpolates between MERA and MPS and can accurately capture long-range quantum correlations even with low-depth networks. Through noisy simulations, we confirm that MERA networks are resilient to noise and typically benefit from additional layers, while additional layers in the generalized MERA may not provide a benefit depending on the noise level and desired correlations.

We conclude by commenting on the extension of these techniques to other tensor networks and future directions. Any tensor network composed entirely of isometric tensors can be simulated holographically, including the recently developed isometric tensor networks in two dimensions that represent nonchiral gapped states [11,14,15,37]. It is not known whether isometric projected entangled pair states can be contracted efficiently, so studying such systems via quantum computers may provide a natural route to quantum advantage [38]. One limitation of the work proposed here is that we optimize the tensor network classically first, and only then convert it to a quantum circuit. While optimizing variational holographic circuits in a hybrid classical-quantum manner has been proposed and explored [6,14,39], it is still an open question on how to do this efficiently, especially as the depth of the circuit increases and while varying the level of noise.

## ACKNOWLEDGMENTS

## APPENDIX A: OPTIMIZATION OF MERA AND GENERALIZED MERA

To prepare the states on the quantum computer, we need a quantum circuit that can be run holographically, so we first classically optimize the MERA and generalized MERA tensor networks. Instead of directly optimizing the MERA and generalized MERA to minimize the energy of the given Hamiltonian, we optimize the networks to have maximal overlap with a reference ground state in the form of a high bond-dimension MPS. Viewing the MERA and generalized MERA as a quantum circuit $U_{\text{(generalized)MERA}}$ that approximates the desired MPS $|\Psi\rangle_{\text{MPS}}$ on $N$ qubits starting from $|O\rangle^{\otimes N}$, we wish to find the circuit such that

$$|||\Psi\rangle_{\text{MPS}} - U_{\text{(generalized)MERA}}|0\rangle^{\otimes N}||_2$$

is minimized. We note that a similar approach has recently been used to convert MPS into brick-wall and sequential quantum circuits [33,34]. While these works did not consider tree tensor network structures, which include MERA and generalized MERA, the general mechanism for optimizing the tensors is similar. Our approach differs in how the initial guesses for the tensors are obtained, which we describe below.

This MPS is found by the density matrix renormalization group (DMRG) algorithm implemented in the TeNPy package [40,41]. A bond dimension $\chi = 256$ is enough to represent the MPS to a very high accuracy for the small systems of $L = 32$ sites. We then subsequently build the MERA and generalized MERA networks by splitting off unitaries and isometries layer by layer as explained below, reducing the remaining physical sites in the MPS by a factor of 2 with each layer. Finally, we optimize this initial guess for the MERA and generalized MERA networks further by iterating over the individual tensors.

### 1. Splitting off a MERA layer

To obtain one layer of the MERA from the MPS of length $L'$, we first perform one sweep left to right, where we split off unitaries acting on every pair of two neighboring sites $2n, 2n + 1$, indexing the sites starting at 1. These unitaries are chosen to disentangle the second Renyi entropy for a cut between the two sites [42]. The found unitaries are used to disentangle the MPS, while their Hermitian conjugates form the unitaries in the layer of the MERA.

Afterwards, we sweep right to left, splitting off the isometries on the other pairs of neighboring sites $2n - 1, 2n$. We form the two-site orthogonality center $\Theta^{\sigma_{2n-1},\sigma_{2n}}_{\alpha_{2n-1},\alpha_{2n+1}}$, indexed by the local basis states $\sigma_{2n-1}, \sigma_{2n}$ on sites $2n - 1, 2n$, and the Schmidt states $\alpha_{2n-1}, \alpha_{2n+1}$ to the left and right, respectively. A singular value decomposition separating the physical indices $\sigma_{2n-1}, \sigma_{2n}$ allows a projection to a new single site $\tilde{\sigma}_n$ and directly yields the corresponding isometry for the MERA layer.

Together, these two steps produce a unitary sublayer of $L'/2 - 1$ tensors and an isometry sublayer of $L'/2$ tensors. We then repeat this process with our new MPS of length $L'/2$ to produce the next layer in the MERA network.

### 2. Splitting of a generalized MERA layer

To produce the generalized MERA layer by layer, we again start with an MPS of length $L'$ in right canonical form. Rather than generate local unitaries and isometries that act on a local pair of sites, we wish to generate "global" unitary and isometry matrix product operators (MPOs) that act on the entire MPS. To do this, we use the Moses Move (MM) algorithm developed in the context of 2D isometric tensor networks [11]. This algorithm splits a two-sided MPS $|\Psi\rangle$ into the product of an isometric MPO $A$ and a new MPS $|\Phi\rangle$, with $|\Psi\rangle \approx A|\Phi\rangle$. By specifying the bond dimensions of the virtual legs between $A$ and $|\Phi\rangle$, $A$ can be either a global unitary or an isometry, while the virtual bond dimension between tensors in $A$ controls how many sites on which each tensor in $A$ can act. We set all bond dimensions of $A$, i.e., both vertical and horizontal bonds in Fig. 2, to 2 so that the produced network can be directly viewed as a quantum circuit of two-site unitary gates. To produce a layer of a generalized MERA, first the MM algorithm is applied to our current MPS of length $L'$ to produce an almost unitary $A$ MPO and a new MPS of length $L' - 1$. The $A$ is almost a unitary, but the last, leftmost tensor in $A_U$ is actually an isometry (projects from an incoming bond dimension of 4 to 2); see the bottom-most row of tensors in Fig. 2, where the leftmost tensor is an isometry. We then use the MM algorithm again to produce an isometric MPO $A_I$ and an MPS of length $L'/2$, where the tensors in $A_I$ alternate between unitaries and isometries. This MPO $A_I$ projects from $L' - 1$ sites to $L'/2$ sites.

A generalized MERA layer is formed by stacking $A_I$ on top of $A_U$ as in Fig. 2. We repeat this procedure to produce the desired number of layers.

### 3. Network optimization

Once the MERA and generalized MERA structures are produced, we optimize the networks by maximizing overlap with the original ground-state MPS of $L$ sites found by DMRG. This is done in a manner similar to the Evenbly-Vidal algorithm of successive polar decompositions for minimizing the energy of a ternary MERA [26]. For the tensor to be optimized, we iteratively form its environment by contracting all tensors in the overlap except for the tensor of interest. We then replace this tensor with the isometric tensor resulting from the polar decomposition of the environment, where the dimensions of the environment determine whether this tensor is a unitary or a projector. Each cycle of this iterative process involves updating each tensor, and we do enough iterations so that the fidelity is no longer meaningfully increasing, e.g., typically 1000 cycles. This produces the optimized finite MERA and generalized MERA networks that we convert into quantum circuits, as discussed in the main paper.

### 4. Conversion to a quantum circuit

Once we have an optimized tensor network, we convert this to a quantum circuit by expanding each isometry into a two-qubit unitary. As noted in the main text, an arbitrary two-qubit $U(4)$ gate can be converted into a sequence of seven single-qubit unitaries specified by 15 angles and three CNOT gates [28]. The circuit diagram for the $U(4)$ gate is shown in Fig. 5. We find these angles by numerically minimizing (via scipy.optimize) the norm of the difference between the desired unitary gate and the unitary gate parameterized by the angles.

In the interior of the MERA, one can exploit the gauge freedom on contracted indices of the MERA to reduce this further to just nine free angles per two-qubit unitary. Essentially, neighboring parameterized gates that act on the same qubits can be combined into a single gate with updated parameters. This can be done as the last generic single-qubit rotation from one gate and the first generic single qubit from the next gate connected by a bond can be combined; hence we can remove two generic single-qubit rotations from each gate (either the first two, last two, or one from each side) in the bulk of the network, removing the need for six angles. For models with charge conservation, the number of free parameters can be reduced even
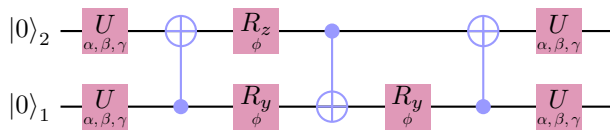
further by enforcing a block-diagonal form of the tensors, similarly as in classical tensor network simulations [16,43].

## APPENDIX B: EXPERIMENTAL DETAILS

The Quantinuum's System Model H1 quantum computer is a trapped-ion system based on a quantum charge-coupled device architecture, where quantum information is stored in the hyperfine "clock" states of $^{171}Yb^+$ ions that can be dynamically moved between different areas of the processor [23]. Each qubit is a pair of a $^{171}Yb^+$ qubit ion and a $^{138}Ba^+$ ion used for sympathetic cooling. Two qubits are paired together to form a four-ion "crystal," with each ion crystal placed in a gate processing zone where single-qubit and entangling two-qubit gates can be applied to both qubits. Ion crystals can be split, moved between gate zones, and merged by dynamical electrical fields created by a cryogenic surface trap. Operations in different gate zones can be done in parallel. The isolation of ion crystals in different zones of the processor lead to long coherence times.

For depth $d = 1$ (2), we run three (two) MERA networks in parallel to obtain the required measurement samples more efficiently. This uses nine (ten) qubits and allows us to reduce quantum computing costs. Furthermore, for depth-($d = 1, 2$) MERA circuits, we do not need to simulate the entire chain of length $L$, as inherently with MERA only a finite range of sites to the right can have nonzero correlations with starting site 10. Hence we simulate up to site 17 for a depth-1 MERA and site 25 for a depth-2 MERA. For depths 3 and 4, the entire chain is simulated as nonzero correlations are possible over the entire chain.

## APPENDIX C: UNITARY NETWORKS

In the main text, we introduced the generalized MERA as a natural interpolation between MERA and MPS networks. Here we provide results for a network ansatz that
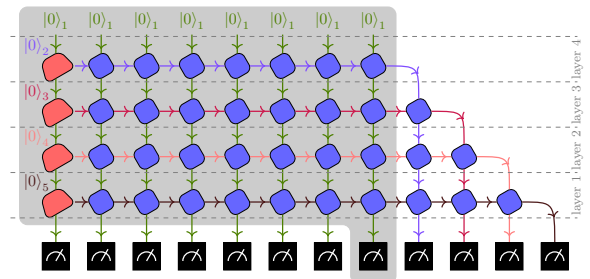


FIG. 6. Isometric representation for the QC-$\ell$ unitary structure of depth 4 for a chain of 12 sites. Five qubits, which are color coded, are required for holographic simulation. The red and blue tensors are isometries and unitaries, respectively. The causal cone for site 8 is shaded in gray, and for a depth-$d$ circuit for a state of length $L$, there are $\mathcal{O}(dL)$ tensors in the causal cone.
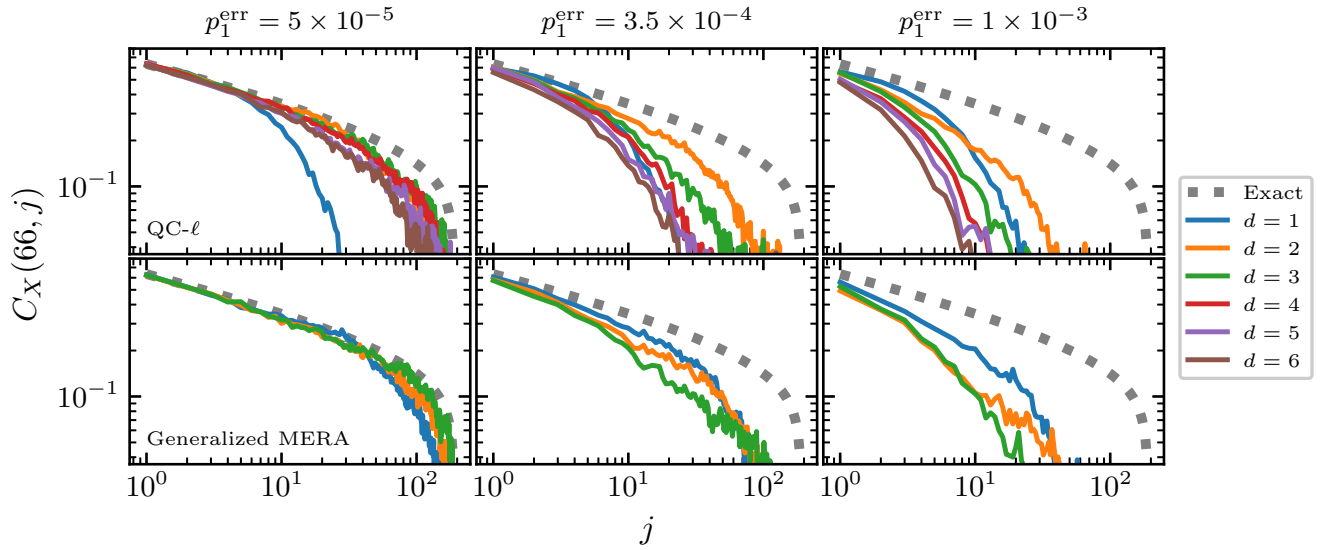


FIG. 5. Decomposition of a generic unitary two-qubit gate $U(4)$ up to a global phase with 15 free angles [28].

FIG. 7. Simulations of $L = 256$ ground states for the unperturbed TFI model realized by QC-$\ell$ (top row) and generalized MERA (bottom, repeat of bottom panel of Fig. 4) networks for different probabilities of depolarizing noise and network depths. Two-qubit error rates are chosen as $p_2^{\text{err}} = 10 p_1^{\text{err}}$. A depth-$d$ QC-$\ell$ circuit requires $d + 1$ qubits compared to the $2d + 1$ needed for MERA and generalized MERA. Note that the QC-$\ell$ networks (shown in Fig. 6) are significantly more affected by noise than the generalized MERA structure due to the larger past causal lightcone for any given site.

can be viewed as a simple quantum circuit analog of an MPS. This ansatz is composed entirely of the global unitary sublayers used in the generalized MERA, as shown in Fig. 6. We label these as QC-$\ell$ networks, following the terminology of Haghshenas *et al.* [12], as they can be viewed as quantum circuits formed by stacking ladder circuits, starting at the rightmost spin and ascending up to the left. These unitary layers should be contrasted with the brick-wall pattern used in MERA. A depth-$d$ QC-$\ell$ network can be collapsed to a $\chi = 2^d$ MPS, where the MPS tensor is formed by collapsing all the tensors in a column.

While the number of gates in a MERA and generalized MERA network for a system of size $L$ asymptotes to $2L$ and $4L$, respectively, as a function of depth $d$, the number of gates in the QC-$\ell$ network scales as $\mathcal{O}(dL)$. This is natural as these circuits do not have the coarse-graining properties of MERA and generalized MERA. As with generalized MERA, a single unitary layer is sufficient to give an infinite range of correlations, but again these correlations decay exponentially. Additionally, the causal cone for a site is extensive and includes all tensors above and to the left, so like generalized MERA, these networks are not suitable for top-down holographic simulation.

The QC-$\ell$ circuits are a generalization of the generalized MERA, as we replace all isometry tensors except for those in the leftmost column with unitaries and add nontrivial tensors to empty sites in the generalized MERA. Thus, the representational power can increase, at the expense of a gate count that scales linearly with depth. Note that a $d = 2$ QC-$\ell$ network and a $d = 1$ generalized MERA are equivalent to one another. We perform noise analysis of

these network in Fig. 7, where we see that QC-$\ell$ networks are more strongly impacted by noise than generalized MERA; a depth-4 QC-$\ell$ and a depth-2 generalized MERA use the same number of qubits, yet the performance of the QC-$\ell$ circuit degrades more significantly with increased noise rates. The performance of higher-depth networks decays quickly with noise, as with approximately $L$ tensors per layer, errors are equally likely in higher layers as in lower layers. Errors in higher layers will affect all tensors to the right and below, even though errors will decay with the correlation length of the state. For MERA and generalized MERA networks, due to the coarse graining, a layer has roughly half as many gates as the layer below it, implying that errors tend to occur lower in the network and thus affect fewer future gates.

## APPENDIX D: ADDITIONAL NETWORK AND CIRCUIT DIAGRAMS

Here we include additional diagrams. First, in analogy with the quantum circuit diagram for MERA shown in
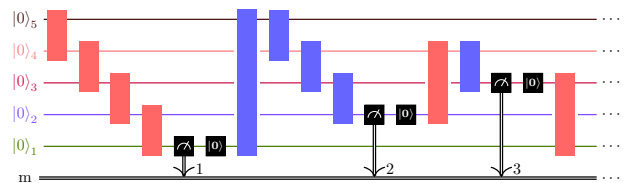


FIG. 8. Quantum circuit for the 12-qubit generalized MERA shown in Fig. 2(a).

Fig. 1(c), in Fig. 8 we show the quantum circuit diagram for the 12-qubit generalized MERA network shown in Fig. 2(a). Again, qubits are measured and reset when available, so the depth-2 network can be holographically simulated with five qubits.

Finally, in Fig. 9 we show depth-4 MERA and generalized MERA networks for 32 qubits so that the pattern for lattices of size $2^\ell$ can be observed. Note that, for both networks, a single layer (consisting of an isometry and unitary sublayer) reduces the number of sites in the effective
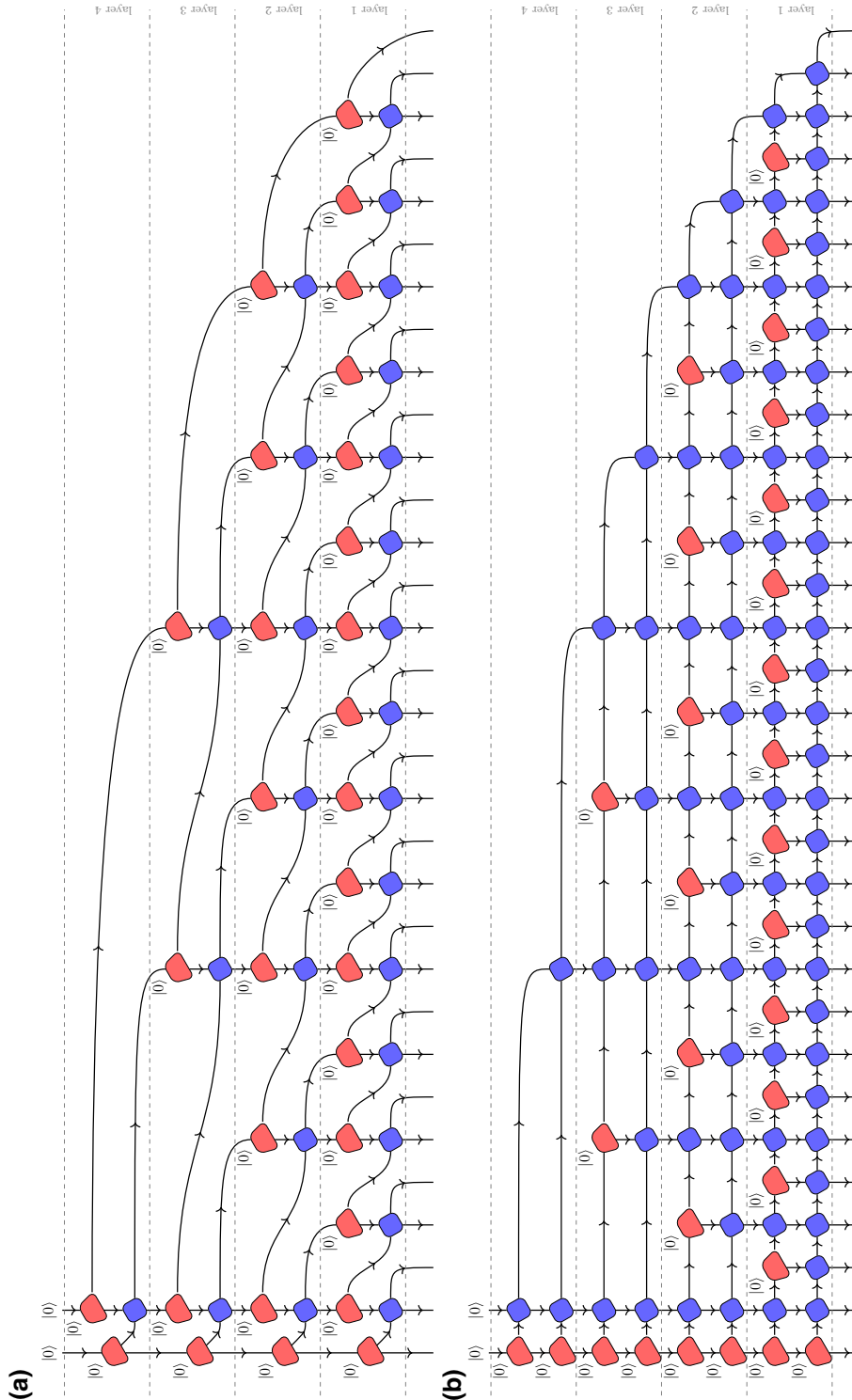


FIG. 9. (a) MERA and (b) generalized MERA network structures for 32 qubits. Red tensors are isometries and act on at least one qubit fixed to be in the initial state $|0\rangle$. Blue tensors are unitary tensors. The diagrams are not particular to $\chi = 2$ tensor networks, even though we use networks of this bond dimension to generate our quantum circuits.

lattice by half, thus performing coarse graining. Consider the generalized MERA structure shown in Fig. 9(b). For an effective lattice of $2^\ell$ sites or qubits, the unitary sublayer consists of $2^\ell - 1$ tensors, $2^\ell - 2$ of which are unitary (blue). The leftmost tensor is an isometry (red), so the unitary sublayer actually removes one site. Then the isometry sublayer reduces the $2^\ell - 1$ sites to $2^{\ell-1}$.

[1] J. Preskill, Quantum computing in the NISQ era and beyond, Quantum **2**, 79 (2018).

[2] C. Schön, E. Solano, F. Verstraete, J. I. Cirac, and M. M. Wolf, Sequential Generation of Entangled Multiqubit States, Phys. Rev. Lett. **95**, 110503 (2005).

[3] I. H. Kim, Holographic quantum simulation. ArXiv:1702.02093 (2017).

[4] I. H. Kim, Noise-resilient preparation of quantum many-body ground states. ArXiv:1703.00032 (2017).

[5] F. Barratt, J. Dborin, M. Bal, V. Stojevic, F. Pollmann, and A. G. Green, Parallel quantum simulation of large systems on small NISQ computers, npj Quantum Inf. **7**, 79 (2021).

[6] M. Foss-Feig, D. Hayes, J. M. Dreiling, C. Figgatt, J. P. Gaebler, S. A. Moses, J. M. Pino, and A. C. Potter, Holographic quantum algorithms for simulating correlated spin systems, Phys. Rev. Res. **3**, 033002 (2021).

[7] This notion of holography is distinct from the notion of correspondences between gravity and holographic field theory.

[8] S. Östlund and S. Rommer, Thermodynamic Limit of Density Matrix Renormalization, Phys. Rev. Lett. **75**, 3537 (1995).

[9] F. Verstraete and J. I. Cirac, Matrix product states represent ground states faithfully, Phys. Rev. B **73**, 094423 (2006).

[10] M. B. Hastings, An area law for one-dimensional quantum systems, J. Stat. Mech.: Theory Exp. **2007**, P08024 (2007).

[11] M. P. Zaletel and F. Pollmann, Isometric Tensor Network States in Two Dimensions, Phys. Rev. Lett. **124**, 037201 (2020).

[12] R. Haghshenas, J. Gray, A. C. Potter, and G. K. L. Chan, The variational power of quantum circuit tensor networks. ArXiv:2107.01307 (2021).

[13] S. H. Lin, R. Dilip, A. G. Green, A. Smith, and F. Pollmann, Real-and Imaginary-Time Evolution with Compressed Quantum Circuits, PRX Quantum **2**, 010342 (2021).

[14] L. Slattery and B. K. Clark, Quantum circuits for two-dimensional isometric tensor networks. ArXiv:2108.02792 (2021).

[15] Z. Y. Wei, D. Malz, and J. I. Cirac, Sequential Generation of Projected Entangled-Pair States, Phys. Rev. Lett. **128**, 010607 (2022).

[16] D. Niu, R. Haghshenas, Y. Zhang, M. Foss-Feig, G. K. L. Chan, and A. C. Potter, Holographic simulation of correlated electrons on a trapped ion quantum processor. ArXiv:2112.10810 (2021).

[17] E. Chertkov, J. Bohnet, D. Francois, J. Gaebler, D. Gresh, A. Hankin, K. Lee, R. Tobey, D. Hayes, B. Neyenhuis, R. Stutz, A. C. Potter, and M. Foss-Feig, Holographic dynamics simulations with a trapped ion quantum computer. ArXiv:2105.09324 (2021).

[18] M. Foss-Feig, S. Ragole, A. Potter, J. Dreiling, C. Figgatt, J. Gaebler, A. Hall, S. Moses, J. Pino, B. Spaun, B. Neyenhuis, and D. Hayes, Entanglement from tensor networks on a trapped-ion QCCD quantum computer. ArXiv:2104.11235 (2021).

[19] G. Vidal, Entanglement Renormalization, Phys. Rev. Lett. **99**, 220405 (2007).

[20] G. Vidal, Class of Quantum Many-Body States That Can Be Efficiently Simulated, Phys. Rev. Lett. **101**, 110501 (2008).

[21] G. Evenbly and G. Vidal, Quantum criticality with the multi-scale entanglement renormalization ansatz. ArXiv:1109.5334 (2013).

[22] G. Evenbly and G. Vidal, Scaling of entanglement entropy in the (branching) multiscale entanglement renormalization ansatz, Phys. Rev. B **89**, 235113 (2014).

[23] J. M. Pino, J. M. Dreiling, C. Figgatt, J. P. Gaebler, S. A. Moses, M. S. Allman, C. H. Baldwin, M. Foss-Feig, D. Hayes, and K. Mayer, et al., Demonstration of the trapped-ion quantum CCD computer architecture, Nature **592**, 209 (2021).

[24] I. H. Kim and B. Swingle, Robust entanglement renormalization on a noisy quantum computer. ArXiv:1711.07500 (2017).

[25] T. J. Sewell and S. P. Jordan, Preparing renormalization group fixed points on NISQ hardware. ArXiv:2109.09787 (2021).

[26] G. Evenbly and G. Vidal, Algorithms for entanglement renormalization, Phys. Rev. B **79**, 144108 (2009).

[27] This is opposite to the convention in tensor network literature where incoming arrows indicate isometry conditions on the tensor.

[28] F. Vatan and C. Williams, Optimal quantum circuits for general two-qubit gates, Phys. Rev. A **69**, 032315 (2004).

[29] N. Moll, P. Barkoutsos, L. S. Bishop, J. M. Chow, A. Cross, D. J. Egger, S. Filipp, A. Fuhrer, J. M. Gambetta, M. Ganzhorn, A. Kandala, A. Mezzacapo, P. Müller, W. Riess, G. Salis, J. Smolin, I. Tavernelli, and K. Temme, Quantum optimization using variational algorithms on near-term quantum devices, Quantum Sci. Technol. **3**, 030503 (2018).

[30] M. Bal, M. M. Rams, V. Zauner, J. Haegeman, and F. Verstraete, Matrix product state renormalization, Phys. Rev. B **94**, 205122 (2016).

[31] D. Radicevic, Spin structures and exact dualities in low dimensions. ArXiv:1809.07757 (2019).

[32] A. Rahmani, X. Zhu, M. Franz, and I. Affleck, Phase diagram of the interacting Majorana chain model, Phys. Rev. B **92**, 235123 (2015).

[33] S. J. Ran, Encoding of matrix product states into quantum circuits of one- and two-qubit gates, Phys. Rev. A **101**, 032310 (2020).

[34] M. S. Rudolph, J. Chen, J. Miller, A. Acharya, and A. Perdomo-Ortiz, Decomposition of matrix product states into shallow quantum circuits. ArXiv:2209.00595 (2022).

[35] We choose this Hamiltonian as the *XX* correlations monotonically decrease rather than oscillate and are thus easier to analyze.

[36] H. Abraham et al. Qiskit: An open-source framework for quantum computing (2019).

[37] T. Soejima, K. Siva, N. Bultinck, S. Chatterjee, F. Poll-
mann, and M. P. Zaletel, Isometric tensor network repre-
sentation of string-net liquids, Phys. Rev. B **101,** 085117
(2020).

[38] N. Schuch, M. M. Wolf, F. Verstraete, and J. I. Cirac, Com-
putational Complexity of Projected Entangled Pair States,
Phys. Rev. Lett. **98,** 140506 (2007).

[39] A. Peruzzo, J. McClean, P. Shadbolt, M. H. Yung, X. Q.
Zhou, P. J. Love, A. Aspuru-Guzik, and J. L. O'Brien, A
variational eigenvalue solver on a quantum processor, Nat.
Commun. **5,** 4213 (2014).

[40] S. R. White, Density Matrix Formulation for Quantum
Renormalization Groups, Phys. Rev. Lett. **69,** 2863 (1992).

[41] J. Hauschild and F. Pollmann, Efficient numerical sim-
ulations with tensor networks: Tensor network Python
(TeNPy), SciPost Phys. Lect. Notes, 5 (2018).

[42] J. Hauschild, E. Leviatan, J. H. Bardarson, E. Altman,
M. P. Zaletel, and F. Pollmann, Finding purifications with
minimal entanglement, Phys. Rev. B **98,** 235163 (2018).

[43] S. Singh, R. N. C. Pfeifer, and G. Vidal, Tensor network
decompositions in the presence of a global symmetry, Phys.
Rev. A **82,** 050301 (2010).